Available online at www.sciencedirect.com
ScienceDirect
Journal of Power Sources 163 (2006) 467–479
JOURNAL OF POWER SOURCES
www.elsevier.com/locate/jpowsour

Performance comparison of two fuel cell hybrid buses with different powertrain and energy management strategies

Minggao Ouyang *, Liangfei Xu, Jianqiu Li, Languang Lu, Dawei Gao, Qicheng Xie

State Key Laboratory of Automotive Safety and Energy, Tsinghua University, Beijing 100084, PR China

Received 25 June 2006; received in revised form 30 August 2006; accepted 15 September 2006
Available online 30 October 2006

Abstract

In order to assess the influences of different powertrain structures and energy management strategies on the performance of hybrid fuel cell buses (FCB), two buses (FCB A and FCB B) were constructed with a "energy hybrid structure" and "power hybrid structure", respectively. Different energy management strategies were investigated based on analysis of the two systems. And the two buses were compared with each other in a bus cycle and constant speed testing. The Polymer Electrolyte Membrane Fuel Cell (PEMFC) in FCB A showed an advantage in fuel economy for it worked usually in the high efficient range of the PEMFC engine. The hydrogen consumption rate in the cycle testing was 7.9 kg/100 km and 9.8 kg/100 km for FCB A and FCB B, and in the 40 kmph constant speed testing it was 3.3 kg/100 km and 4.0 kg/100 km, respectively. The fuel economy could be improved when the hydrogen and air supply subsystems are optimized and controlled with an advanced algorithm. It could also benefit from a braking energy regeneration system. Compared with FCB A, the PEMFC in FCB B worked under unfavorable operation conditions because its working range was comparatively wide, and the power changing rate was relatively large from a statistical point of view, which resulted in performance recession of the PEMFC in FCB B. After a mileage of 7000 km, the output power of the PEMFC in FCB B was reduced by 10%, compared with 2.4% in FCB A. An advanced energy management strategy is necessary to split the power between the PEMFC and a battery suitable for long durability of a PEMFC.

Keywords: Fuel cell hybrid bus; PEMFC; Energy management strategy; Fuel economy; Performance degradation

1. Introduction

Polymer Electrolyte Membrane Fuel Cell (PEMFC) vehicles have been considered as one way to sustainable development in the world because of their high efficiency, zero emission and low noise. The fuel economy of a PEMFC vehicle is projected to be 2.5–2.7 times the fuel economy of a conventional gasoline internal combustion engine vehicle (ICEV) on the same platform [1]. However, the PEMFC vehicles have the disadvantages of high price and a short life time, which makes commercialization difficult.

The vehicle can be equipped with a pure PEMFC system or a hybrid system. No energy storage system (ESS) is applied in a pure fuel cell vehicle, therefore the PEMFC suffers overloads and drastic load changing. But in the hybrid fuel cell vehicle, both the PEMFC and the ESS are utilized as energy sources and it is possible to operate the fuel cell under more efficient conditions. The life-cycle cost is greatly affected by the cost of the fuel cell, hydrogen and other components. The cost of a fuel cell vehicle is reduced by hybridization [2].

The fuel economy of a hybrid vehicle is affected by the driving conditions, energy management strategy, etc. An advanced control algorithm will have to be incorporated into the vehicle development processes to achieve good drivability and high fuel economy [3]. As introduced in [3], there was a possible 2–3% increase in fuel economy when implementing a stochastic dynamic energy management strategy.

Many kinds of hybrid powertrain structures are available now. In order to access the influences of different powertrain structures on vehicle performance, two fuel cell buses (FCB), FCB A

* Corresponding author. Tel.: +86 10 62773025; fax: +86 10 62785708.
E-mail address: ouymg@tsinghua.edu.cn (M. Ouyang).

0378-7753/$ – see front matter © 2006 Elsevier B.V. All rights reserved.
doi:10.1016/j.jpowsour.2006.09.033

Nomenclature

F	Faraday constant, 96485.3415 s A mol^{-1}
I	current (A)
m	mass (g)
M	molecule mass (g mol^{-1})
P	power (W)
Q	battery capacity (C)
soc	the value of state of charge
T	temperature (°C)
Tr	torque (N m)
U	voltage (V)
U_{bus}	bus voltage, the voltage at the input port of DC/AC inverter (V)

Greeks letters

Δ	change in ...
η	efficiency
ω	rotational speed (rad s^{-1})
ψ	pedal position

Superscripts and subscripts

auxiliary	auxiliary components
battery	battery
cell	single cell of PEMFC
charging	the charging process of the bi-directional DC/DC converter
dcac	the DC/AC converter for the traction motor
dcdc	the DC/DC converter
discharging	the discharging process of the bi-directional DC/DC converter
fc	PEMFC
high	upper limit value
hydrogen	hydrogen
low	lower limit value
max	maximum value
min	minimum value
motor	traction motor
utilized	utilization coefficient
*	request value

and FCB B were constructed with "energy hybrid structure" and "power hybrid structure", respectively. The two structures are defined according to the hybridization rate of the bus. In "energy hybrid structure" the hybridization rate is relatively high and the ESS should be able to meet a high requirement for energy, while the hybridization rate in "power hybrid structure" is relatively low and only a high requirement for power should be met by the ESS.

This work was part of the project of "Research and development of Fuel Cell City Bus" in China, which belongs to the tenth five-year "863" program—the hi-tech research and development program of the country. The project was undertaken by the Department of Automotive Engineering in Tsinghua University together with other companies and institutes from the year 2002 to 2005, during which the PEMFC system was studied and several fuel cell hybrid buses were constructed and tested.

2. Powertrain structure

A PEMFC system, a DC/DC converter, a battery and a traction motor are included in both of the two powertrain structures, shown as in Fig. 1(a and b).

As shown in Fig. 1(a), there are three modules in "energy hybrid structure", the PEMFC system with a DC/DC converter, the traction motor with a DC/AC inverter and the battery. The energy consumed by the motor is provided by the PEMFC and the battery. The DC/DC converter is adopted to regulate the output power of the PEMFC.

The three modules contained in the "power hybrid structure" are the PEMFC system, the battery with a bi-directional DC/DC converter and a traction motor with a DC/AC inverter, as in Fig. 1(b). Charging/discharging the battery could be controlled by the bi-directional DC/DC converter [4].

2.1. PEMFC system

The PEMFC is regarded as the heart of a hybrid vehicle because it consumes hydrogen to produce energy and occupies a large share of the whole vehicle's cost. Generally the PEMFC must be capable of meeting the power needs under sustainable driving conditions. The vehicle power requirement could be calculated according to the vehicle dynamics. The results indicate that a power of at least 60 kW is needed in a cruise with a velocity of 60 kmph, and the maximum power requirement in accelerating is nearly 120 kW. Then a PEMFC system with a rated power of 65 kW is chosen for FCB A, and additional power needed in accelerating could be provided by the ESS. The rated power of PEMFC and the battery are almost same, then this powertrain structure is named as "energy hybrid structure". Another PEMFC system in FCB B is selected with a rated power of 100 kW, since it is connected to the motor directly and the peak power requirement is higher than that in FCB A. The rated power of PEMFC is much larger than that of the battery in FCB B, then this powertrain structure is called "power hybrid structure". Table 1 shows the main parameters of the two PEMFC systems. The PEMFC in FCB A contains two stacks and the one in FCB B contains three stacks. The PEMFC stacks are connected in parallel.

Table 1
PEMFC parameters

	FCB A	FCB B
Stack number	2	3
Rated power (kW)	65	100
Overload power (kW)	88	130
Output voltage (V)	330–450	330–450
Noise level (dB)	<80	82–88

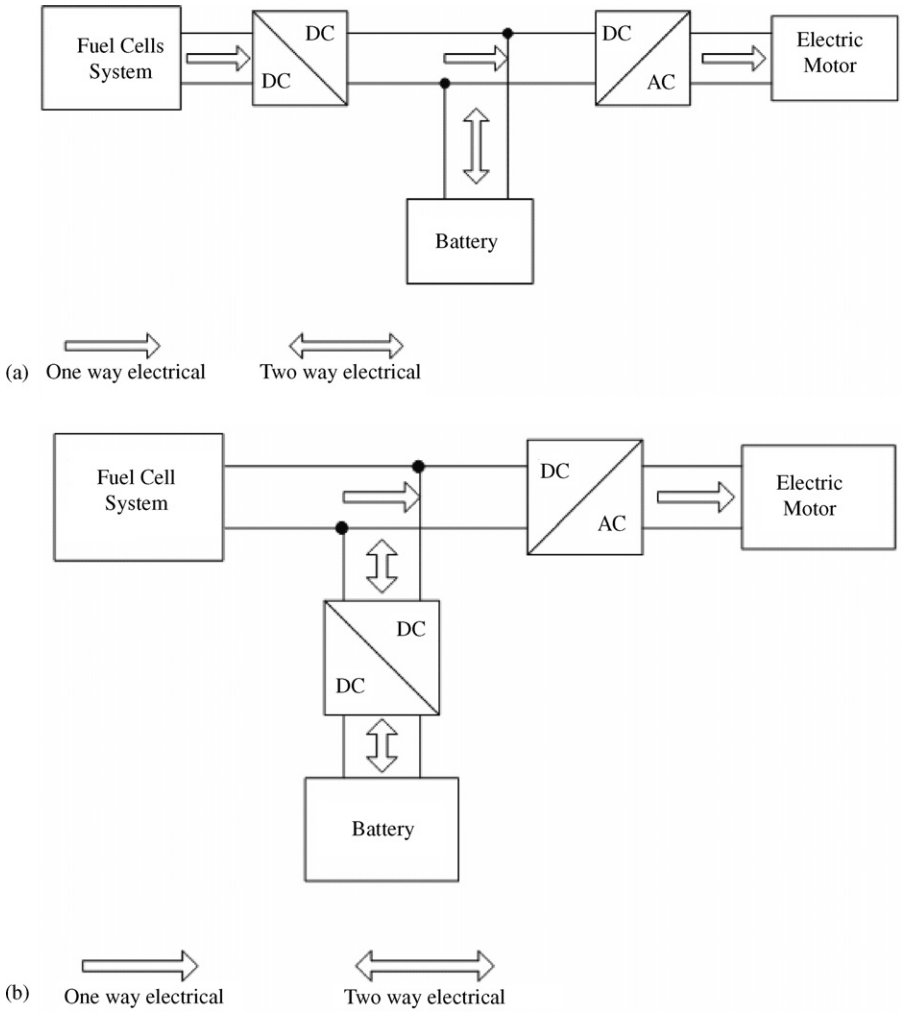

Fig. 1. (a) Energy hybrid structure and (b) power hybrid structure.

2.2. ESS

As the second power source, the ESS plays an important role in the whole system. It provides the vehicle with boost power when accelerating and stores part of the energy when decelerating or idling. For FCB A, a lead-acid battery with an amp-hour rating of 80 Ah was utilized. The ESS in FCB B was linked to the motor by a DC/DC converter, so a Ni-MH battery with an amp-hour rating of 80 Ah was used. Table 2 presents the parameters.

2.3. Motor

The traction motors in the two buses were produced by the same company with a rated power of 120 kW, which was enough to meet the power requirement in a bus route. The motor was integrated with a DC/AC inverter and a motor controller. The axle torque was controlled by the controller according to its rotational speed and the pedal position. Table 3 indicates some main parameters of the motor and Fig. 2 presents the relationship between the maximum motor torque and the axle speed.

2.4. DC/DC converter

A single directional DC/DC converter was applied in FCB A because the PEMFC only outputs energy, and a bi-directional converter in FCB B was selected because the ESS needs to be charged and discharged, shown in Table 4. A DC/DC converter with a rated power of 90 kW has been selected to match with the PEMFC system in FCB A. For the bi-directional DC/DC

Table 2
ESS parameters

	FCB A	FCB B
Type	Lead-acid battery	Ni-MH battery
Amp-hour rating (Ah)	80	80

Table 3
Motor parameters

Parameter	Value
Rated power (kW)	120 (at 1800 rpm)
Maximum speed (rpm)	7000

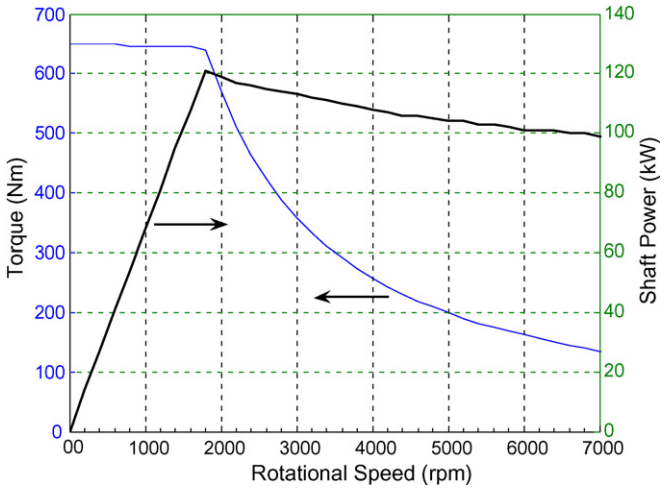

Fig. 2. Motor torque and power vs. speed.

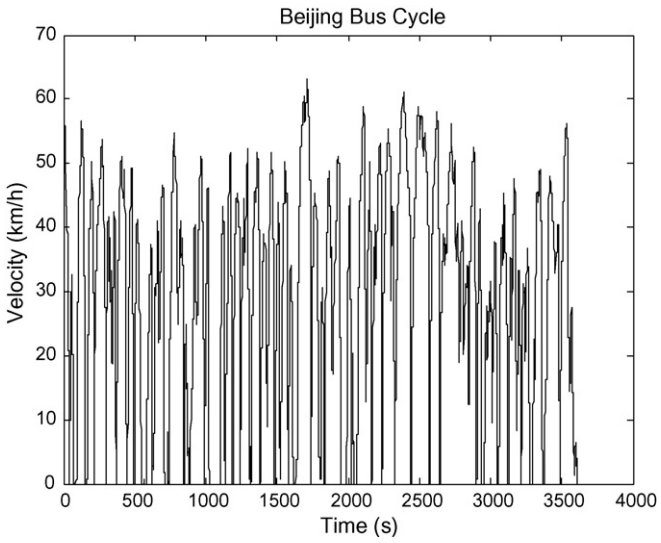

Fig. 3. Typical Beijing Bus Cycle.

Table 4
DC/DC parameters

	FCB A	FCB B
Type	Single directional, buck	Bi-directional
Rated power (kW)	90	50/20

converter in FCB B, the rated power is 50 kW in boost mode and 20 kW in buck mode, which was matched with discharging and charging states of the battery.

3. Energy management strategy

The pedal position and motor axle speed were measured and transmitted to the motor controller, which determined the output power of the traction motor. The power requirement of the motor was distributed by the energy management strategy between the PEMFC and the ESS to obtain high fuel economy, long life time and good vehicle performance. Energy management strategy should satisfy following requirements in the bus cycle testing, as presented in Fig. 3:

(i) to minimize the hydrogen consumption;
(ii) to keep the power output of the PEMFC in a suitable range;
(iii) to limit the PEMFC power changing rate;
(iv) to maintain the state of charge (soc) of ESS in a narrow scope.

The hydrogen consumption should be minimized in the cycle testing to achieve a high fuel economy. The PEMFC should work in a concentrated range and its power changing rate should be restricted, otherwise there will be negative influence on the PEMFC life time, which is discussed in Section 4.3.1. The ESS should be kept in a narrow scope so as to be able to supply the boost power during accelerating at any time.

The PEMFC and the ESS were connected with each other through a DC/DC converter, which is considered as the key element in the energy management strategy. The DC/DC module, including a DC/DC converter and its controller, operated in two modes. One was in the current-control mode, where the output current is controlled. The other was in the voltage-control mode, where the output voltage of the DC/DC was under control. The DC/DC converters could be classified into three categories, the buck converters, the boost converters and the buck–boost converters. The output voltage was lower than the input value in the buck converter, while it was higher than the input value in the boost converter [5,6].

The DC/DC converter in the "energy hybrid structure" works in the current-control mode. Then the energy could be accurately distributed in FCB A because the DC/DC current is controlled to the target value, which is calculated according to the power requirement from the traction motor. The bi-directional DC/DC converter works in the voltage-control mode, and its operation mode could be changed between buck mode and boost mode. The battery is charged when the bi-directional DC/DC operates in buck mode, and it is discharged in boost mode.

3.1. Energy management strategy in FCB A

In the "energy hybrid structure" the DC/DC converter is connected between the PEMFC and the traction motor. The converter operates in current-control mode and its target current is determined by the energy management strategy.

The bus voltage and state of charge (soc) of the battery are two important variables here. The bus voltage, which is the voltage at the input port of the DC/AC inverter of the traction motor, could be measured directly. And the battery soc, which is the ratio of the available capacity of the battery to the nominal value, could be estimated by a number of mathematical methods, as presented in [7]. The battery charging/discharging power is determined by Eq. (2). The power demanded by the motor is calculated considering the motor rotational speed and pedal position from Eq. (1). The difference between the power demanded by motor and the charging/discharging power of the battery is the power requirement for the DC/DC converter as described in Eq. (3). With the measured bus voltage, the target current of the DC/DC is

calculated by Eq. (4). Function g describes the relation between the target current of the DC/DC converter and its actual current in Eq. (5). Normally if the vehicle power requirement can be fulfilled, then $g(x) = x$, otherwise $g(x) < x$. Eq. (6) calculates the actual power output to the DC/AC inverter of the motor.

The hydrogen consumption rate is calculated in Eq. (9), where the PEMFC output power P_{fc} shown as in Eq. (8) consists of two parts. One is the part output to the DC/DC converter and the other is the parasitic power by the auxiliary components of the PEMFC system, such as the air management system. Eq. (10) shows the relation of the battery soc to other variables.

As listed above from (i) to (iv), the PEMFC output power, the power changing rate, the hydrogen consumption and the soc value should be optimized with the assistance of computer simulation. Two functions should be determined in the energy management strategy in FCB A, the driver command function $T^*_{r,motor}(\omega_{motor}, \psi)$ and the battery charging/discharging function $f(soc)$. The first function forecasts the motor torque output based on the motor speed and pedal position. And the second determines the charging/discharging power of the battery at a certain soc value. Energy is distributed according to the motor power requirement, which is calculated based on the result of driver command function. Experiments were arranged to determine the driver command function. And the battery charging/discharging function was optimized in the bus cycle testing as introduced in Section 4.1. Fig. 4(a and b) illustrates the results of the two functions.

The motor torque decreases with increase of its rotational speed, and it grows with the increase of the pedal position, shown as in Fig. 4(a). And in Fig. 4(b) the battery soc is designed to maintain around a nominal value of 0.8. When the value of soc is smaller than 0.8, the battery is charged. And it is discharged in other cases. The power requirement for the DC/DC converter can be calculated according to Fig. 4(a) and Eqs. (1)–(3). A first-order delay loop is utilized when calculating the PEMFC target power in order to limit its changing rate, as shown in Fig. 4(c). Then if power requirement for PEMFC increases rapidly to a constant level, the actual output power increases in an exponential curve gradually.

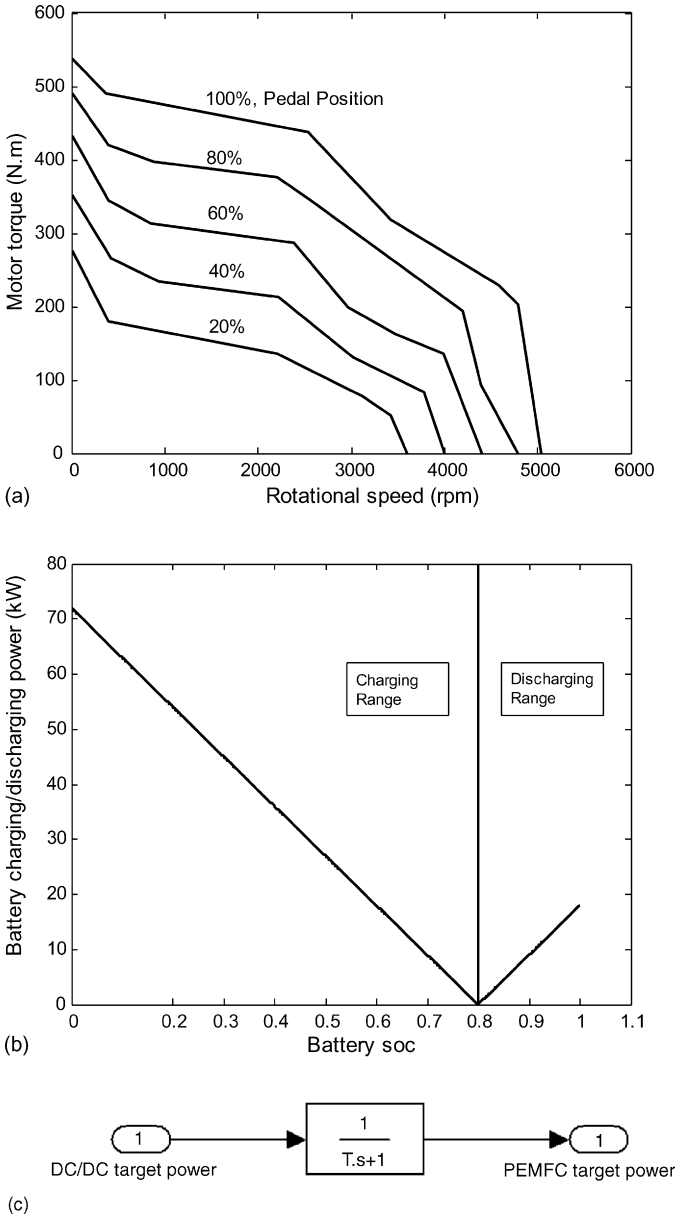

Fig. 4. (a) Driver command explanation, (b) ESS charging/discharging function and (c) a first-order delay loop between DC/DC target power and PEMFC target power.

3.2. Energy management strategy in FCB B

In the "power hybrid structure" the bi-directional DC/DC converter is connected between the ESS and the traction motor. The energy flow direction through the DC/DC converter is changed by switching the operation modes based on the bus voltage, which is the same as the PEMFC output voltage in this case. The energy management strategy determines the values of the bus voltage for switching the modes.

System description and management strategy in FCB B is simpler than those in FCB A due to less variables related. Because the power requirement of the motor has no relation to the strategy, it cannot be distributed accurately between the PEMFC and the ESS.

The battery output voltage is controlled by the DC/DC converter in the buck mode. Its output power is a function of the output voltage, temperature and the soc value shown as in Eq. (12). Then the PEMFC output power can be calculated by Eq. (13).

The PEMFC output voltage is controlled by the DC/DC converter in the boost mode. Ignoring the change of the PEMFC polarization curve in transient processes, the PEMFC output power could be considered as a function of bus voltage and stack temperature, shown as in Eqs. (14)–(16) determine the ESS power and the value of soc.

The energy management strategy described above should also satisfy the requirements listed in 3. The strategy changes the energy flow direction based on the value of the bus voltage. If the bus voltage decreases below a certain value $U_{bus,low}$, which means the power demanded by the motor grows over the upper limit, then the PEMFC output voltage is set to $U_{fc,min}$ and the bi-

directional DC/DC converter operates in the boost mode to make the battery be discharged, as presented in Eq. (17). The variable $U_{fc,min}$ defined as the inflexion point on the PEMFC polarization curve is the minimum fuel cell voltage allowed in the powertrain system during operation. If the bus voltage grows over the value $U_{bus,high}$, which means the motor power requirement decreases below the lower limit, then the output voltage of the battery is set to the open circuit voltage $U_{battery,max}$ and the DC/DC converter switches to the buck mode to charge the battery as shown in Eq. (18).

The four voltages were adjusted in experiments and the final values are as below:

$$U_{bus,low} = 335\,V, \quad U_{bus,high} = 360\,V,$$
$$U_{fc,min} = 325\,V, \quad U_{battery,max} = 255\,V$$

4. Performance comparison

With different structures and energy management strategies, the two buses were compared with each other in the bus cycle testing and 40 kmph constant speed testing.

4.1. Testing conditions

Fig. 3 indicates the condition of the bus cycle testing. It is a typical urban city route in Beijing with a maximum speed of 60 kmph, where accelerating, decelerating and idling state appear alternately. Generally, accelerating process occupies 53% of the whole period, decelerating occupies 36% and idling occupies 11%. The performances of the two buses during the three transient processes and the energy flow in the powertrain are analyzed in the following section.

4.2. Powertrain performance

4.2.1. Accelerating

The acceleration performance of the two FCB was measured according to Chinese national standard. The results were 24 s and 27.86 s from 0 kmph to 50 kmph for FCB A and FCB B, respectively. An accelerating process in the bus cycle testing is selected to compare the powertrain performance of the two buses. The energy distribution between the PEMFC and the ESS is presented in Fig. 5(a and b).

The power requirement of the traction motor was similar. It increased rapidly in the first several seconds and decreased gradually after reaching the peak point. As referred in Section 3.1, the energy requirement in FCB A could be accurately distributed and a first-order delay loop was used when calculating the PEMFC target power. Therefore, the PEMFC power grew gradually when the requirement increased suddenly in the first several seconds. The rest of the power was supplied by the ESS, which grew rapidly at first and decreased gradually to a constant level. Without the protection of the DC/DC converter, the ESS output power contained a high frequency portion as in Fig. 5(a). In this process, the PEMFC offered 59% and the battery provided 41% of the motor energy requirement.

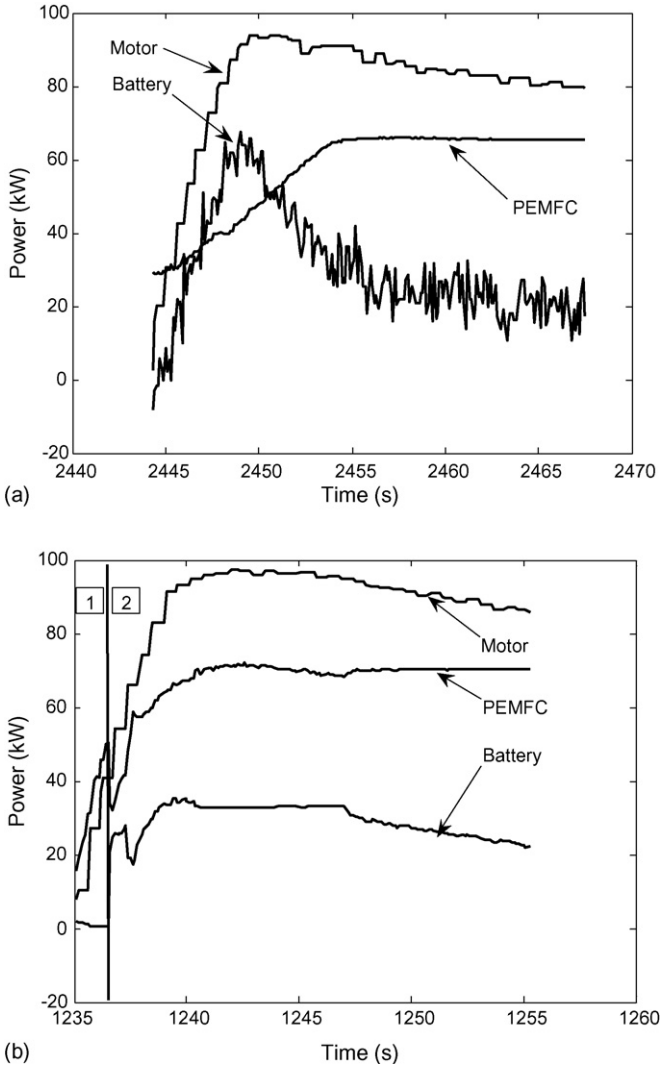

Fig. 5. Energy distribution during accelerating in: (a) FCB A and (b) FCB B.

The process of FCB B contained two stages, as in Fig. 5(b). In the first 1.5 s the bi-directional DC/DC converter operated in the buck mode, so the battery could not output energy. The PEMFC output power was a little larger than what was demanded by the motor because of the parasitic power in the PEMFC system. After about 1.5 s the bus voltage was smaller than the specified value, then the bi-directional converter switched to the boost mode and the battery could be discharged. PEMFC offered 65% of the total energy and the ESS provided the rest 35%. Protected by the bi-directional converter, the ESS operated mildly with a smaller maximum power output.

4.2.2. Decelerating

Fig. 6(a and b) presents the energy distribution in the two buses when they decelerated from 50 km h^{-1} to 0 km h^{-1} in 17 s for FCB A and 16 s for FCB B.

Since braking energy regeneration system has not yet been applied in the two buses, the traction motor was disconnected with the braking system when the vehicle decelerated. Then it operated in an idling state with a small requirement power. The

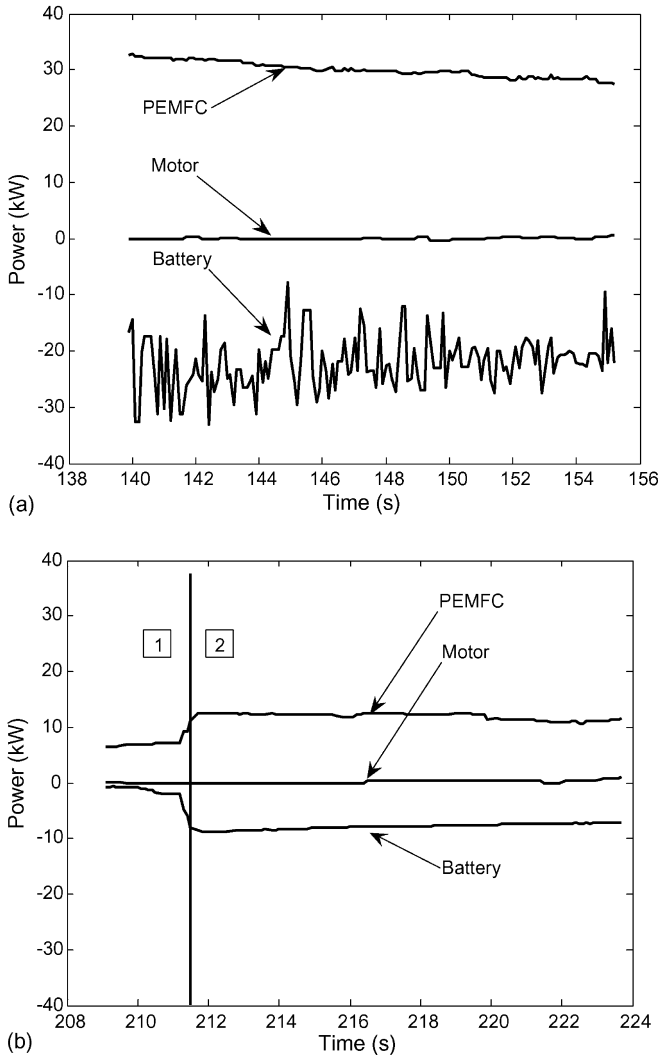

Fig. 6. Energy distribution during decelerating in: (a) FCB A and (b) FCB B.

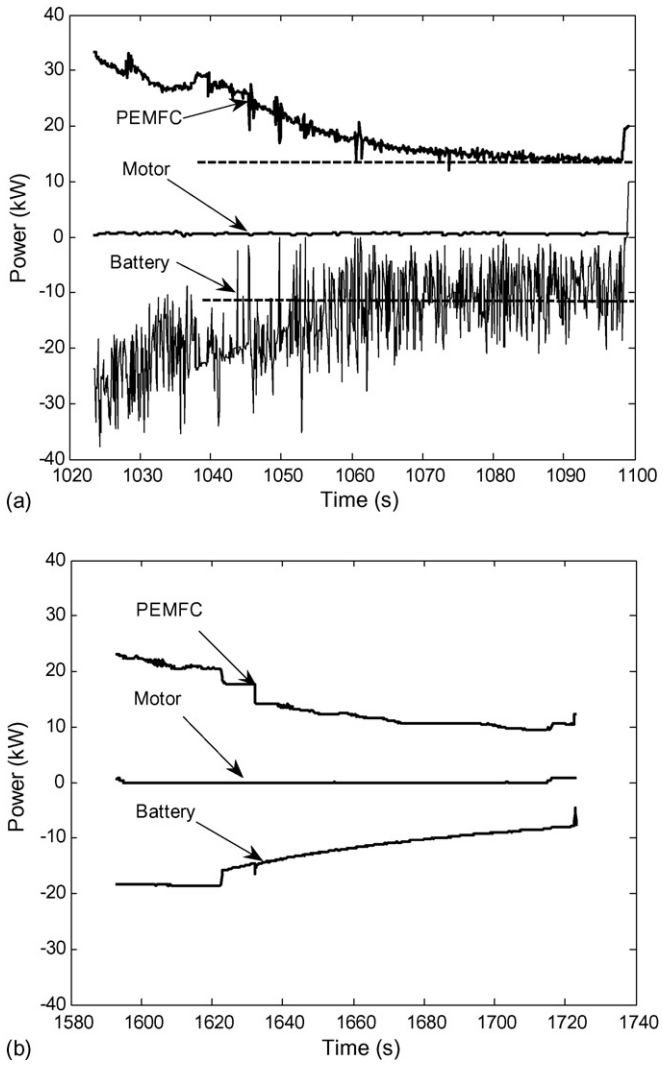

Fig. 7. Energy distribution during idling state in: (a) FCB A and (b) FCB B.

battery was charged and the auxiliary components were driven by the PEMFC.

In FCB A the DC/DC target power could be calculated by Eqs. (2) and (3). Battery soc rose because of charging. The battery charging power decreased with the increase of soc, as presented in Fig. 4(b). The PEMFC output power became smaller with the decrease of the battery requirement at the same time.

The process in FCB B could also be separated into two stages. In the first stage the bi-directional DC/DC converter operated in boost mode and the battery could not be charged. After the bus voltage was higher than the specified value $U_{bus,high}$, the converter switched to the buck mode and the battery could be charged.

4.2.3. Idling

The vehicle stopped in idling state and the output power of the traction motor was zero. Fig. 7(a and b) indicates the energy distribution in idling state.

The PEMFC worked in the same way as in decelerating process. The output power of PEMFC decreased in an exponential curve gradually to 12.6 kW, which was calculated by Eq. (2). Because the idling state appeared after decelerating, the bi-directional DC/DC converter in FCB B operated in the buck mode all the time.

4.2.4. Energy flow in the powertrain

Fig. 8(a–d) indicates the energy flows in the two buses on average in the testing. Fig. 8(a and b) are for FCB A and (c and d) for FCB B. Fig. 8(a and c) is about the bus cycle testing and (b and d) about the 40 kmph constant speed testing. The fuel power/energy is calculated according to the low heat value (LHV) of the hydrogen. The input fuel energy is regarded as 100%. All the losses and energy transmitted to the traction motor were calculated.

Defined as (net engine power)/(fuel power), the PEMFC engine efficiency reached 55% in the bus cycle testing in FCB A, as in Fig. 8(a). 2.31% of the fuel energy was consumed by the Fuel Cell Engine auxiliary components. The energy losses in Fuel Cell Stacks were as much as 42.69%, including the losses in stacks and through the purge valve. The hydrogen cannot be 100% utilized in a real PEMFC system. The utilization coefficient may reach 90% normally, but it plummets to a low level

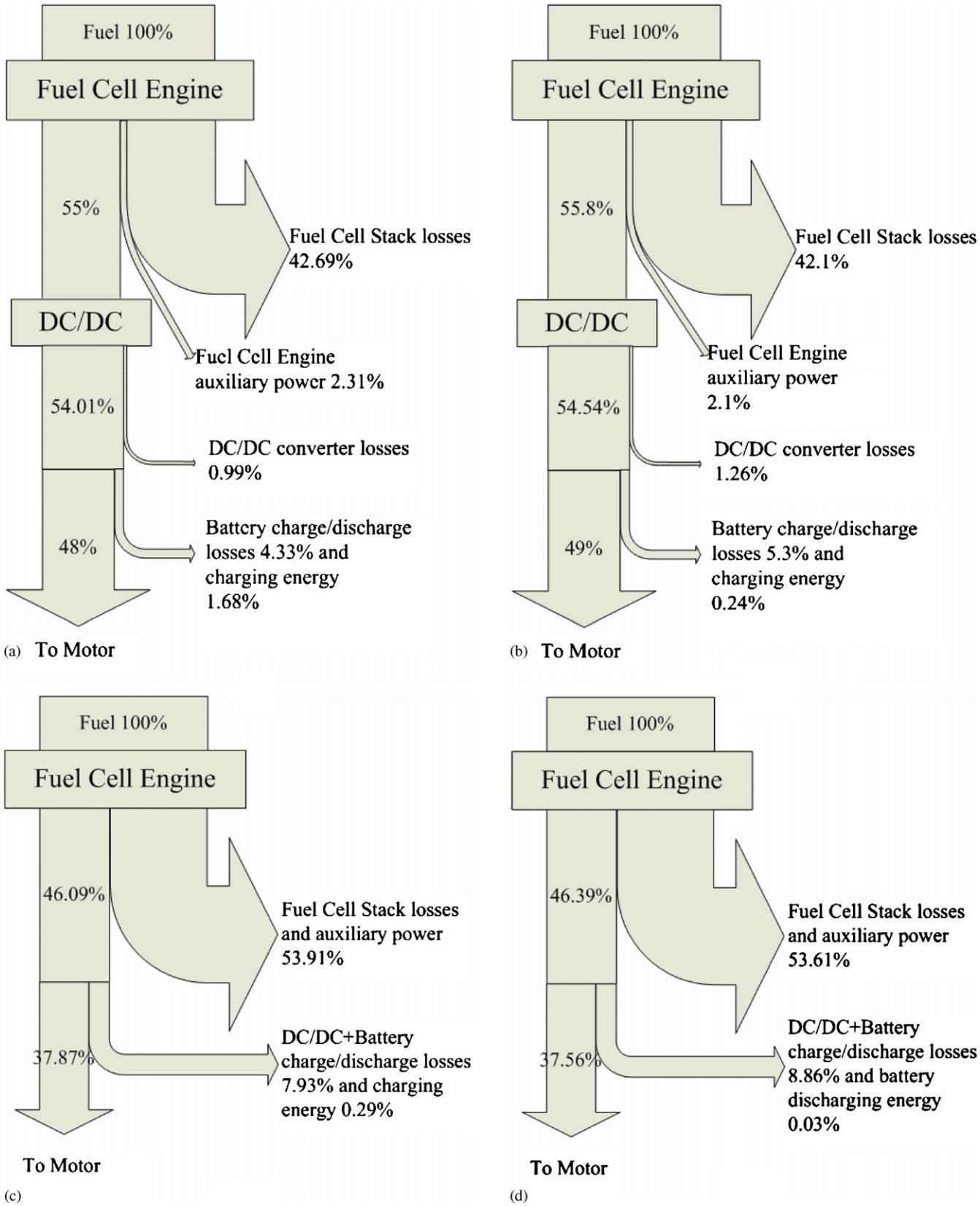

Fig. 8. Energy flow diagram of: (a) FCB A in cycle testing, (b) FCB A in 40 kmph constant speed testing, (c) FCB B in cycle testing and (d) FCB B in 40 kmph constant speed testing.

in idling or low power requirement states, because the hydrogen has to go out through the purge valve to take the water out of the anode. However, this part of energy losses could be reduced based on an optimized purge-valve control strategy. The DC/DC converter loss and the battery charge/discharge loss were 0.99% and 4.33%, respectively. Finally there was 48% of the fuel energy transmitted to the traction motor and 1.68% was stored in the ESS.

The PEMFC engine efficiency reached 55.8% in the 40 kmph constant speed testing, which was higher than that in the bus cycle testing in FCB A, as shown in Fig. 8(b). Both of the Fuel Cell Engine auxiliary power and the stack losses were reduced. The average power requirement in 40 kmph constant speed testing was lower than the one in bus cycle testing, leading to the reduction of Fuel Cell Engine auxiliary power. And the PEMFC in constant speed testing worked more stably than in bus cycle testing, therefore the fuel utilization coefficient was higher. Finally 49% of the fuel energy was transmitted to the motor and the ESS was charged by 0.24% of the total fuel energy.

Fig. 8(c and d) presents results in FCB B. In the bus cycle testing the PEMFC engine efficiency was 46.09% and there was 37.87% of the total fuel energy transmitted to the traction motor, as in Fig. 8(c). These two values were lower than those in FCB A. Reason for this is the different working points of the two PEMFCs in the two buses, which is discussed in detail in Section 4.3.1. The Fuel Cell Stack losses and auxiliary power were 53.91%, and the battery charging/discharging losses were 7.93%. Here the battery charging/discharging losses contained the losses in the bi-directional DC/DC converter. Finally there was 0.29% of the fuel energy stored in the battery.

As shown in Fig. 8(d), due to a more stable operation condition in 40 kmph constant speed testing, the PEMFC engine efficiency was higher than in the bus cycle testing, 46.39% versus 46.09%. The Fuel Cell Stack losses and auxiliary power were 53.61%, and the battery charging/discharging losses were 8.86%. 0.03% of the fuel energy was stored in the battery.

Comparing Fig. 8(a–d), there were only slight differences in the Fuel Cell Engine efficiency and energy transmitted to the traction motor for one bus in the two testing. This is because

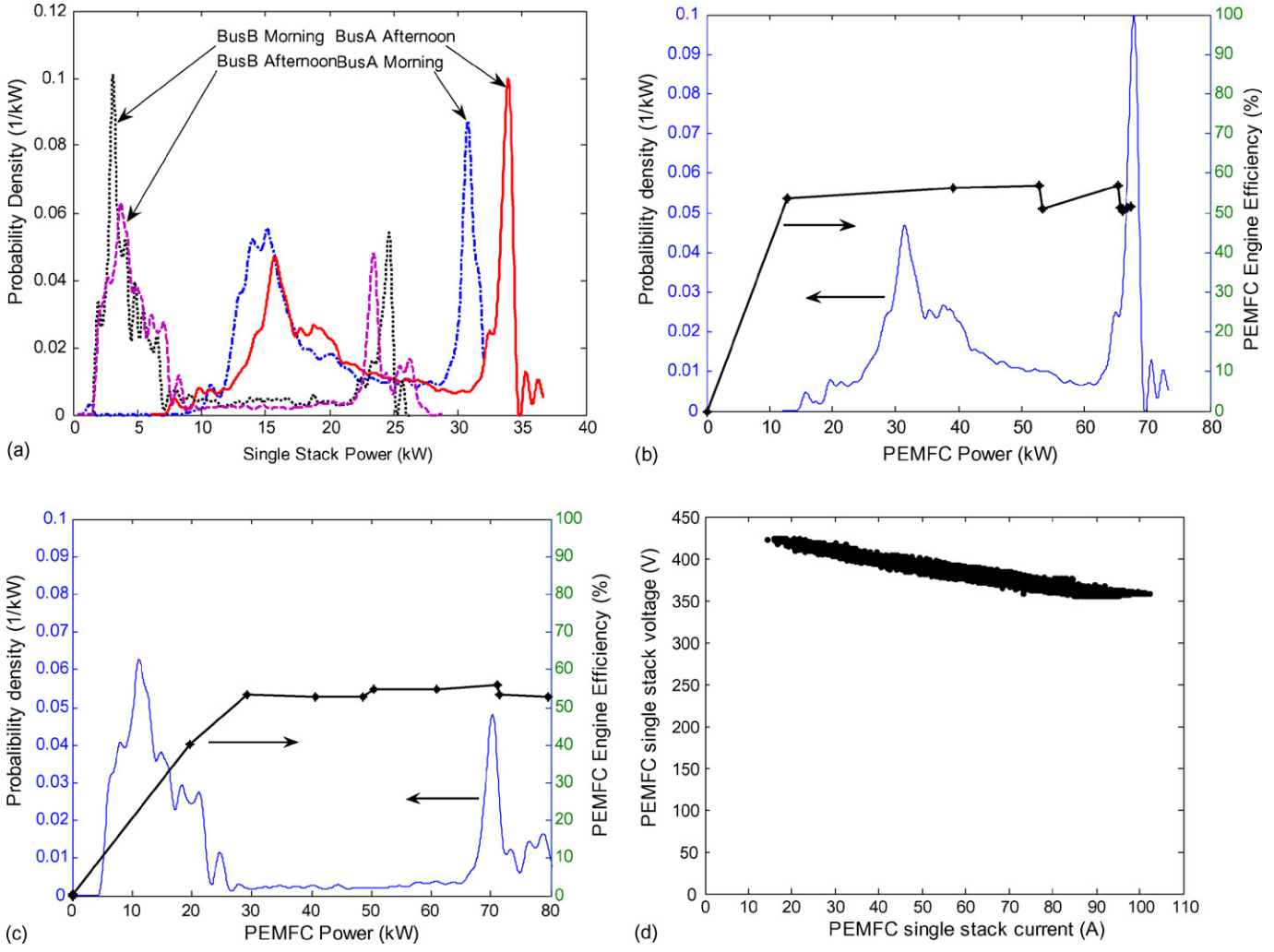

Fig. 9. (a) Single stack power probability density, (b) PEMFC power probability density and steady efficiency in FCB A, (c) PEMFC power probability density and steady efficiency in FCB B, (d) PEMFC single stack working points distribution in FCB A, (e) PEMFC single stack working points distribution in FCB B, (f) single stack power changing rate probability density, (g) single stack polarization curve and (h) PEMFC performance recession.

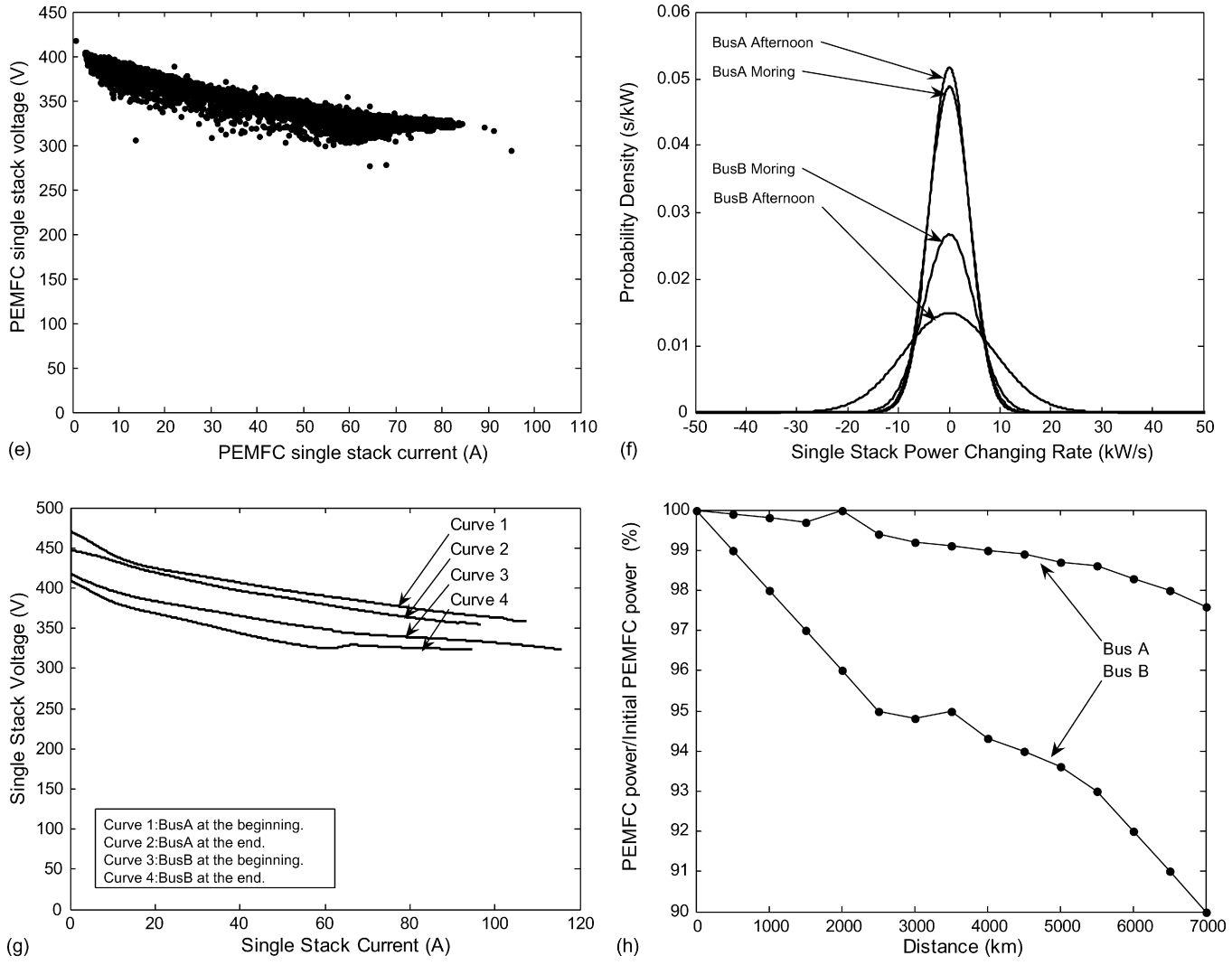

Fig. 9. (*Continued*).

the Fuel Cell Engine efficiency changes little in a wide range of PEMFC net power. As in Fig. 9(b), the PEMFC engine efficiency in FCB A keeps almost constant in 12–70 kW. And this is 30–80 kW in FCB B, as shown in Fig. 9(c). Besides, the hydrogen consumption rate increases almost linearly with the increase of PEMFC power, it differs a lot for one FCB in bus cycle testing and constant speed testing, as presented in Table 5.

Ideally there is no benefit to a hybrid under constant load when the vehicle velocity is kept at a constant speed accurately. But in reality the vehicle velocity was controlled by the driver, therefore it could not be at 40 kmph strictly but changed in a small range. The vehicle velocity of FCB A was between 38 kmph and 42 kmph and of FCB B it was between 36 kmph and 44 kmph. The small transient processes resulted in differences in the constant speed testing.

Different powertrain structures determine different working points of the PEMFCs, which finally result in the engine efficiency difference. Generally speaking, the PEMFC engine efficiency was about 55% in FCB A and 46% in FCB B both in bus cycle testing and constant speed testing. As referred in [8], the maximum theoretical efficiency of PEMFC is as high as 83% at 25 °C. And if the fuel utilization coefficient could reach 90%, the PEMFC engine efficiency would be 75%. But such high efficiency is never reached. Simulation results from [4] show that the PEMFC engine efficiency could be between 57.5% (FCHEV) and 60.5% (stand-alone FCEV).

Table 5
Vehicle performance

	FCB A	FCB B
Maximum speed (km h^{-1})	69.4	72.1
Hydrogen consumption rate at 40 kmph constant speed testing (kg/100 km)	3.3	4.0
Hydrogen consumption rate in standard cycle testing (kg/100 km)	7.9	9.8

The power consumed by the air management system represents the largest parasitic loss in the Fuel Cell system [1]. And the capacity of the air management system determines the minimum cell voltage that can be reached [9]. Besides, part of the hydrogen goes out through the purge valve in idling or low power requirement states. Therefore, the efficiency of the PEMFC engine could be improved by applying an advanced controller for the hydrogen and air supply system.

What's more, the fuel economy could also be improved by applying a braking energy regeneration system. As a simulation result in [4], the hydrogen input energy calculated using LHV was 3236 Wh, and there was 552 Wh regenerated from braking energy. By using a braking energy regeneration system, the efficiency jumped from 57.5% to 74.6% with the assistance of the ESS.

4.3. Components performance

The bus cycle testing shown in Fig. 3 is made up of large numbers of transient processes. The differences in transient processes result in distinct performances of the components in the two buses.

4.3.1. PEMFC performance

Fig. 9(a–h) has been constructed to illustrate the performances of the PEMFCs in the bus cycle testing.

Fig. 9(a) presents the probability density of the single PEMFC stack power in the morning and in the afternoon. The two peaks on each curve stands for the two main working points of the PEMFC. The peak with higher power emerged when the bus accelerated, and the peak with lower power appeared when the bus decelerated or stopped. The figure shows that the PEMFC in FCB B operated more often in a lower power range than the one in FCB A. The peaks on the curve moved rightwards in the afternoon, which means the bus operated more frequently in a higher power range with a higher environment temperature. The maximum value of the single stack power in FCB A was about 37 kW, compared with 28 kW in FCB B. The load for a single stack in FCB B was lower than that in FCB A since there were more stacks in FCB B.

The PEMFC engine efficiency was measured in steady state in the lab, which is presented in Fig. 9(b and c). It starts from zero and increases to a steady value with the increase of the PEMFC power. The transient efficiency in the bus cycle was different from the one measured in steady state, however, it could be regarded as a reference. Both of the curves of PEMFC engine efficiency and PEMFC power probability density have been drawn in Fig. 9(b and c). It is clear that the PEMFC in FCB A worked in the high efficient range while in FCB B it operated mainly in the low efficient range. This is the reason why FCB B showed a lower PEMFC engine efficiency on average in the bus cycle testing than FCB A. Then it could be concluded that FCB A should have a higher fuel economy. This conclusion is further confirmed by the data in Table 5, where the hydrogen consumption rate was 7.9 kg/100 km in FCB A and 9.8 kg/100 km in FCB B. The advantage in fuel economy of FCB A also appeared in the 40 kmph constant speed testing, where the hydrogen consumption rate was 3.3 kg/100 km in FCB A and 4.0 kg/100 km in FCB B. Additionally, as shown in Table 5, FCB B could reach a higher maximum speed, since the rated power of the PEMFC in FCB B was larger. The PEMFC operated in the low power and high efficiency condition in the constant speed testing, so the average vehicle hydrogen consumption rate was less than half of that in the bus cycle testing.

Fig. 9(d and e) presents the working points of the PEMFC stacks. The distribution of working points for one stack in FCB A was more concentrated than that in FCB B. The working range for one cell in FCB B was wider than in FCB A.

The four curves in Fig. 9(f) indicate the normal distribution of the single stack power changing rate. 99.4% of the points of FCB A in the afternoon were located between $-10\,\mathrm{kW\,s^{-1}}$ and $10\,\mathrm{kW\,s^{-1}}$, while only 73.7% were located in the same scope in FCB B. The average absolute value of single stack power changing rate in the afternoon was $3.68\,\mathrm{kW\,s^{-1}}$ in FCB A, and it was $6.06\,\mathrm{kW\,s^{-1}}$ in FCB B. And in the morning when the environment temperature was low, the average absolute value of single stack power changing rate in FCB B was also higher than the value in FCB A, $3.68\,\mathrm{kW\,s^{-1}}$ and $3.44\,\mathrm{kW\,s^{-1}}$, respectively.

Since the PEMFC in FCB B operated in a wider range and with a higher power changing rate than the one in FCB A, the performance degradation of the PEMFC in FCB B was larger. Fig. 9(g) compares the polarization curves for the single stacks of the two buses at the beginning and at the end of a driving distance of about 7000 km in the bus cycle route.

It should be mentioned that the maximum cell voltage at the beginning of 7000 km testing was 470/496 = 0.95 V in FCB A, and 425/472 = 0.9 V in FCB B. Such difference should have influence on the fuel economy. But the difference is slight and difficult to evaluate, so that the influence was ignored here.

Fig. 9(h) presents the performance recession more clearly. The output power of the two PEMFCs was measured when the single stack current was 100A. If the initial power was regarded as 100%, after the long driving distance the power of PEMFCs was reduced by 2.4% in FCB A and 10% in FCB B.

The powertrain configuration and the energy management strategy in FCB B determined the unfavorable operation condition for the PEMFC and led to a great performance recession. In order to improve the durability of the PEMFC engine, a modified energy management strategy is necessary to split the power requirement in a suitable way.

4.3.2. Battery performance

As referred in Section 4.2 the ESS in FCB A suffered a drastic fluctuant power requirement in transient processes, which results in a more uniform diagram in Fig. 10(a) than in Fig. 10(b). What's more, the battery in FCB A supplied a much larger power than the one in FCB B during accelerating referred in Section 4.2.1, the maximum power of the battery in FCB A was as much as 80 kW, and it was only 40 kW in FCB B. After the bus cycle testing the battery in FCB A was charged with 1.33 kWh, occupying 1.42% of the hydrogen energy. And the battery in FCB B was charged with 0.18 kWh, which was 0.24% of the total energy input. The energy charged into the battery could be further utilized.

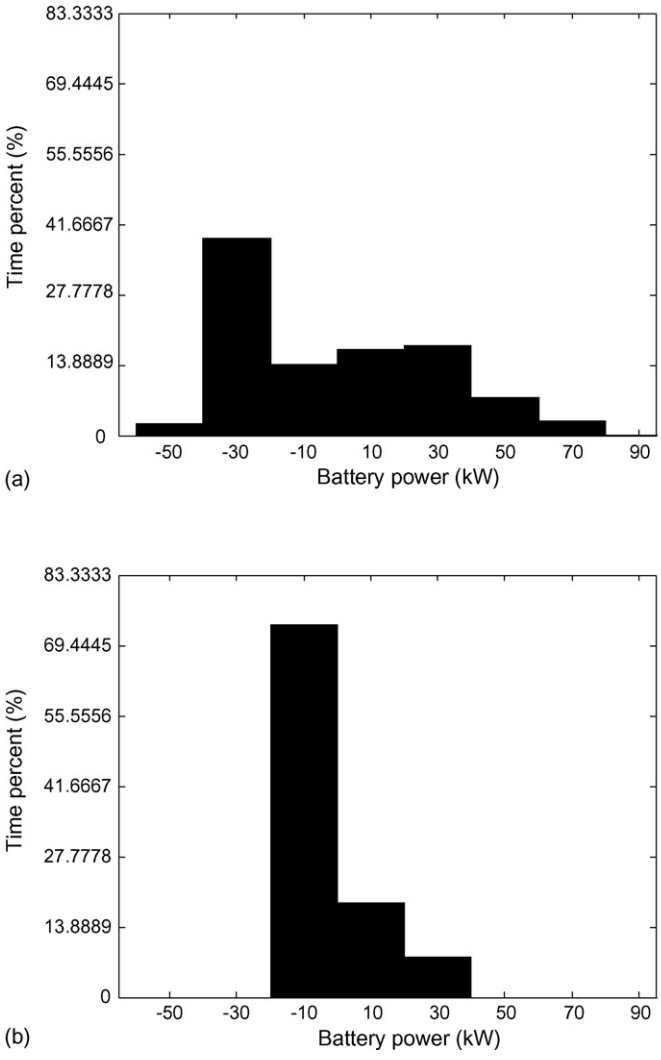

Fig. 10. Battery performance in cycle testing in: (a) FCB A and (b) FCB B.

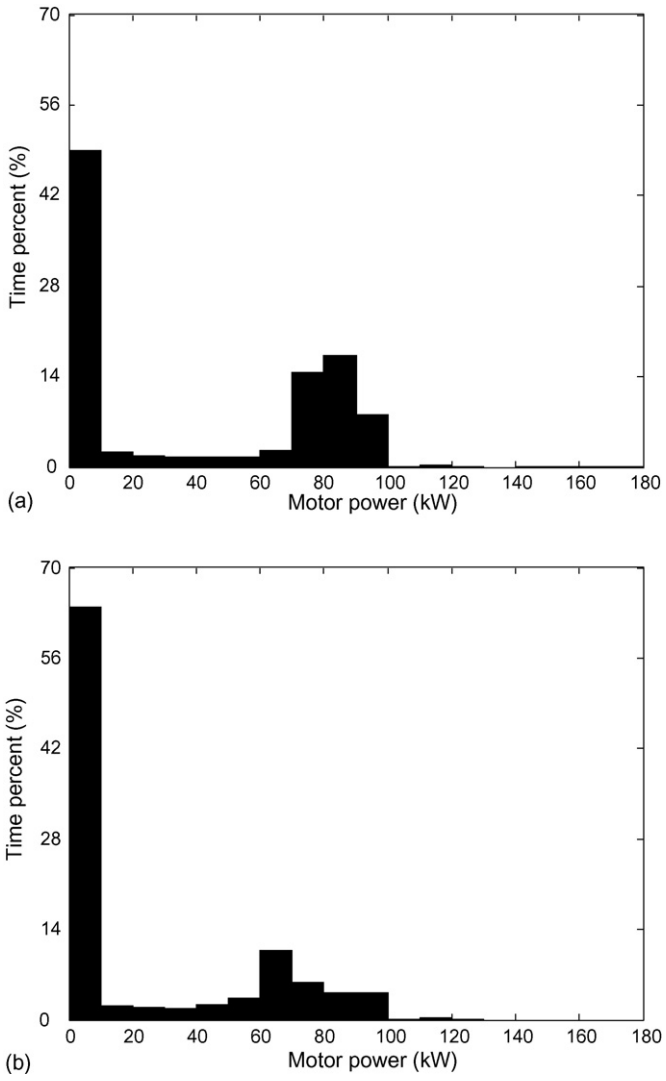

Fig. 11. Motor performance in cycle testing in: (a) FCB A and (b) FCB B.

4.3.3. Motor performance

The motor performances of the two buses in bus cycle testing are compared in Fig. 11(a) and (b). The similar distributions of traction motor power can be observed. The largest part of the working points located in the range of small power, where the motor efficiency was low. The low power appeared when the vehicle decelerated, which occupied about 47% of the whole period of the testing. When the vehicle accelerated, the motor power increased to the value between 60 kW and 100 kW.

The average input power of the two motors in the bus cycle testing were different, which were 38.7 kW for FCB A, and 29.1 kW for FCB B. Since the motor input power came from the PEMFC and ESS, it indicated that the power-following characteristic which mainly determined by the powertrain architectures and hybridization strategies, was different in two cases. In addition, the two buses ran at different time, therefore the traffic conditions were not same, e.g. different start–stop time, the different driving habits of two drivers might also have some influence on the motor power.

5. Conclusions

Powertrain structures and energy management strategies have a great influence on the fuel economy of the FCB and the life time of the PEMFC. As discussed above, FCB A with an "energy hybrid structure" and FCB B with a "power hybrid structure" showed differences in fuel economy, performance recession, etc.

The PEMFC in the "power hybrid structure" provided a larger power than the one in the "energy hybrid structure" when the power demand increases suddenly. This was demonstrated in the accelerating process as in Fig. 5(a and b), where the output power of the PEMFC in FCB A increased more slowly under the control of the DC/DC converter. The power distributions between the PEMFC and the ESS in decelerating and idling were similar in the two buses since there was no braking regeneration system.

With the "energy hybrid structure" and an energy management strategy based on the current-control method of the DC/DC converter, the PEMFC in FCB A operated in a highly efficient range in bus cycle testing. The PEMFC engine efficiency was 55% on average in FCB A and 46% on average in FCB B in

the bus cycle testing and 40 kmph constant speed testing. The PEMFC engine efficiencies were similar for one FCB in two different testing conditions, because the efficiency changes little in a wide range of PEMFC net power, as in Fig. 9(b and c). As the PEMFC in FCB A worked in the range with a high efficiency, FCB A showed an advantage in fuel economy with a hydrogen consumption rate of 7.9 kg/100 km, compared with 9.8 kg/100 km in FCB B in bus cycle testing. The higher fuel economy of FCB A was also demonstrated in the 40 kmph constant speed testing, where the hydrogen consumption rate was 3.3 kg/100 km in FCB A and 4.0 kg/100 km in FCB B. The fuel economy could be further improved by a braking energy regeneration system and an advanced controller for the hydrogen and air supply system.

With the "power hybrid structure" and an energy management strategy based on the voltage-control method of the DC/DC converter, the performance of the PEMFC in FCB B declined quickly due to its wide working range and high power changing rate on the Beijing Bus Route. The output power of the PEMFC in FCB B was reduced by 10% after a mileage of about 7000 km on the Beijing Bus Route, however, it was only 2.4% in FCB A. An advanced energy management strategy is therefore necessary to split the energy in a much better way to protect the PEMFC and achieve a long life time.

Appendix A

Equations for system description and energy management strategy in the "energy hybrid structure" of FCB A.

$$P^*_{\mathrm{dcac}} = \frac{\omega_{\mathrm{motor}} T^*_{\mathrm{r,motor}}(\omega_{\mathrm{motor}}, \psi)}{\eta_{\mathrm{motor}}} \tag{1}$$

$$P^*_{\mathrm{battery}} = f(\mathrm{soc}) \tag{2}$$

$$P^*_{\mathrm{dcdc}} = P^*_{\mathrm{dcac}} - P^*_{\mathrm{battery}} \tag{3}$$

$$I^*_{\mathrm{dcdc}} = \frac{P^*_{\mathrm{dcdc}}}{U_{\mathrm{bus}}} \tag{4}$$

$$I_{\mathrm{dcdc}} = g(I^*_{\mathrm{dcdc}}) \tag{5}$$

$$P_{\mathrm{dcac}} = \frac{\omega_{\mathrm{motor}} T_{\mathrm{r,motor}}}{\eta_{\mathrm{motor}}} \tag{6}$$

$$P_{\mathrm{battery}} = P_{\mathrm{dcac}} - P_{\mathrm{dcdc}} \tag{7}$$

$$P_{\mathrm{fc}} = \frac{U_{\mathrm{bus}} I_{\mathrm{dcdc}}}{\eta_{\mathrm{dcdc}}} + P_{\mathrm{auxiliary}} \tag{8}$$

$$\Delta m_{\mathrm{hydrogen}} = \int_0^t \frac{P_{\mathrm{fc}} M_{\mathrm{hydrogen}}}{2\eta_{\mathrm{utilized}} F U_{\mathrm{cell}}}\,\mathrm{d}t \tag{9}$$

$$\mathrm{soc} = \mathrm{soc}_0 + \int_0^t \frac{P_{\mathrm{battery}}}{U_{\mathrm{bus}} Q}\,\mathrm{d}t \tag{10}$$

Equations for system description and energy management strategy in the "power hybrid structure" of FCB B.

$$P_{\mathrm{dcac}} = \frac{\omega_{\mathrm{motor}} T_{\mathrm{r,motor}}}{\eta_{\mathrm{motor}}} \tag{11}$$

$$P_{\mathrm{battery}} = P(U_{\mathrm{battery}}, T_{\mathrm{battery}}, \mathrm{soc}) \tag{12}$$

$$P_{\mathrm{fc}} = \frac{P_{\mathrm{dcac}} - P_{\mathrm{battery}}}{\eta_{\mathrm{dcdc,charging}}} + P_{\mathrm{auxiliary}} \tag{13}$$

$$P_{\mathrm{fc}} = P_{\mathrm{fc}}(U_{\mathrm{bus}}, T_{\mathrm{fc}}) \tag{14}$$

$$P_{\mathrm{battery}} = \frac{P_{\mathrm{dcac}} - P_{\mathrm{fc}} + P_{\mathrm{auxiliary}}}{\eta_{\mathrm{dcdc,discharging}}} \tag{15}$$

$$\mathrm{soc} = \mathrm{soc}_0 + \int_0^t \frac{P_{\mathrm{battery}}}{Q U_{\mathrm{battery}}}\,\mathrm{d}t \tag{16}$$

$$\text{When } U_{\mathrm{bus}} \le U_{\mathrm{bus,low}}, \quad U^*_{\mathrm{bus}} = U_{\mathrm{fc,min}} \tag{17}$$

$$\text{When } U_{\mathrm{bus}} > U_{\mathrm{bus,high}}, \quad U^*_{\mathrm{battery}} = U_{\mathrm{battery,max}} \tag{18}$$

References

[1] R.K. Ahluwalia, X. Wang, A. Rousseau, R. Kumar, J. Power Sources 130 (2004) 192–201.
[2] K.S. Jeong, B.S. Oh, J. Power Sources 105 (2002) 58–65.
[3] A. Schell, H. Peng, D. Tran, E. Stamos, C.-C. Lin, M.J. Kim, Annu. Rev. Control 29 (2005) 159–168.
[4] R.K. Ahluwalia, X. Wang, A. Rousseau, J. Power Sources 152 (2005) 233–244.
[5] I. Gadoura, K. Zenger, T. Suntio, P. Vallittu, Telecommunications Energy Conference (INTELEC '99), Copenhagen, Denmark, 1999, pp. 449–454.
[6] Y.B. Shtessela, A.S.I. Zinoberb, I.A. Shkolnikovc, Automatica 39 (2003) 1061–1067.
[7] S. Piller, M. Perrin, A. Jossen, J. Power Sources 96 (2001) 113–120.
[8] J. Larminie, A. Dicks, Fuel Cell System Explained, second ed., John Wiley & Sons Ltd, England, 2003, p.25.
[9] R.K. Ahluwalia, X. Wang, J. Power Sources 139 (2005) 152–164.